Chiral and critical spin liquids in a spin-1/2 kagome antiferromagnet

W. Zhu, S. S. Gong, and D. N. Sheng

Phys. Rev. B **92**, 014424 — Published 28 July 2015

DOI: 10.1103/PhysRevB.92.014424

Chiral and critical spin Liquids in spin-$1/2$ kagome antiferromagnet

W. Zhu, S. S. Gong, and D. N. Sheng
Department of Physics and Astronomy, California State University, Northridge, California 91330, USA

The kagome spin-1/2 systems have attracted intensive attentions in recent years as the primary candidate for hosting different gapped spin liquids (SL). To uncover the nature of the novel quantum phase transition between the SL states, we study a minimum XY model with the nearest neighbor (NN) (J_{xy}), the second and third NN couplings ($J_{2xy} = J_{3xy} = J'_{xy}$). We identify the time reversal symmetry broken chiral SL (CSL) with the turn on of a small perturbation $J'_{xy} \sim 0.06 J_{xy}$, which is fully characterized by the fractionally quantized topological Chern number and the conformal edge spectrum as the $\nu = 1/2$ fractional quantum Hall state. Interestingly, the NN XY model ($J'_{xy} = 0$) is shown to be a critical SL state adjacent to the CSL, characterized by the gapless spin singlet and spin triplet excitations. The quantum phase transition from the CSL to the gapless critical SL is driven by the collapsing of the neutral (spin singlet) excitation gap. The effect of the NN spin-z coupling J_z is also studied, which leads to a quantum phase diagram with an extended regime for the gapless SL.

PACS numbers: 73.43.Nq, 75.10.Jm, 75.10.Kt

I. INTRODUCTION

The spin liquid (SL) is an exotic state of matter which escapes from forming the conventional orders even at zero temperature[1]. Different from a featureless insulator, a gapped SL develops a topological order[2–4] with fractionalized quasiparticles encoded in the long-range entanglement of system[5]. The SL physics may play a fundamental role for understanding strongly correlated systems and unconventional superconductivity[6–21]. There have been intensive studies of SL in frustrated magnetic systems, however, the discovery of SL has been rare in the past. A few frustrated magnetic systems on square and honeycomb lattices have been proposed as the candidates for gapped topological SL[22–25], but further studies find that the competing plaquette valence-bond solid may dominate the magnetic disorder region[26–29].

Interestingly, the nearest neighbor (NN) dominant spin-$1/2$ kagome Heisenberg model has been identified to host a gapped SL based on the state of art density matrix renormalization group (DMRG) calculations[30–33], where a near quantized topological entanglement entropy[34,35] has been found consistent with a Z_2 SL[32,33]. The topological degeneracy as a signature evidence for such a gapped topological state[2,8–10,36] has not been fully established, while different methods have been applied to tackle this problem[31,37]. Meanwhile, the variational studies find that the Dirac gapless SL has the lower variational energy among different states[38,39]. The nature of the SL in the kagome Heisenberg model remains not fully understood.

By introducing the second- and third- NN couplings for the spin-$1/2$ kagome systems[40], DMRG studies[41,42] discover the Kalmeyer-Laughlin CSL theoretically predicted more than 20 years ago[43–47], which spontaneously breaks time reversal symmetry (TRS) and is identified as the $\nu = 1/2$ fractional quantum Hall (FQH) state[43,44,48]. Interestingly, the CSL state is also found in the spin anisotropic kagome model involving the second and third NN xy-plane couplings[49], or by introducing the TRS breaking three-spin chirality interactions[50]. However, the nature of the quantum phase transition, especially how the quantum state and entanglement spectrum (ES) evolve near such a transition have not been addressed. We do not know what a physical mechanism can drive the quantum phase transition in such a system, and if the emergence of the previously identified gapped SL for the NN kagome Heisenberg model has close connection with the collapsing of the CSL[51]. Our work is motivated to address these open questions.

Along with theoretical developments, experiments also discover different promising SL candidates in the triangular organic compounds[52–54] and kagome antiferromagnets Herbertsmithite and Kapellasite $Cu_3Zn(OH)_6Cl_2$ in recent years[55–60]. These materials appear to have gapless excitations as revealed by the specific heat and neutron scattering measurements[56–59]. Thus, it would be extremely interesting to also search for some minimum spin-$1/2$ kagome model which can host a gapless SL. Our calculation indicates that the kagome spin XY model is a suitable starting point for such a purpose, as the XY-plane interactions may help to realize the gapless vortex liquid through the fractionalization of vortices[61–63].

In this paper, we address the quantum phase diagram and the nature of the collapsing of CSL in kagome spin system based on DMRG and exact diagonalization (ED) calculations. We study the spin-$1/2$ XXZ kagome model with extended XY interactions[49], which is the promising candidate for a gapless SL. As shown in the inset of Fig. 1(a), the spin-XY model Hamiltonian is given as

$$\begin{aligned} H &= (J_{xy}/2)\sum_{\langle i,j\rangle}(S_i^+S_j^- + h.c.) + J_z\sum_{\langle i,j\rangle} S_i^zS_j^z \\ &+ (J'_{xy}/2)\sum_{\langle i,j\rangle'}(S_i^+S_j^- + h.c.), \end{aligned} \tag{1}$$

where the summations are taken over the NN $\langle i,j\rangle$, the second and third NN $\langle i,j\rangle'$ couplings. We set $J_{xy} = 1$ as energy scale. We also set the equal second- and third-neighbor couplings as we find interesting topological phases are stabilized around that region[64]. Our main results are summarized as the phase diagram in Fig. 1(a). First of all, for the XY model with $J_z = 0$, we establish a CSL for $J'_{xy} \gtrsim 0.06$ based on the topological features of the state which include the conformal chiral edge spectrum in accordance with the $\nu = 1/2$ FQH

state and the topological quantized Chern number $C = 1/2$. We also find the robust chiral long range correlation for the CSL phase based on finite size scaling of wider systems. We identify the physical driving force for the destruction of the CSL as the collapsing of the singlet excitation gap with reducing J'_{xy}. Following the evolution of ES, we find that the phase transition takes place through the coupling between the low-lying entanglement states with opposite chiralities, which naturally leads to a critical state with TRS and gapless neutral excitations[65,66]. Our results represent a significant progress in understanding the connection between different SLs[49] by identifying the mechanism of the phase transition and establishing the characteristic nature of the critical SL phase adjacent to the CSL.

We use DMRG[67] and ED to study cylinder and torus systems with the geometry shown in the inset of Fig. 1(a). The number of sites in cylinder (open boundary condition in the x-direction) or torus system is $N = 3 \times L_y \times L_x$ with L_x and L_y as the numbers of unit cell in the x and y directions[68]. We perform the flux insertion simulations on cylinder systems based on the newly developed adiabatic DMRG to detect the topological Chern number[41]. In DMRG studies we keep up to $8000 - 10000$ states for most of the simulations for accurate results. For the gapless SL regime, the convergence becomes difficult, where we mainly present spin excitation gap which is well converged as it only depends on the average local bond energy.

The remaining of the paper is organized as following: In Sec. II, we present the evidence of CSL in the phase diagram, including the measurements of spin-spin correlation, chiral-chiral correlation and characteristic edge mode counting from entanglement spectrum. In Sec. III, we determine the phase boundary using the fractional Hall conductance (Chern number). In Sec. IV, we study the response of of the entanglement spectrum to a flux inserting in the cylinder geometry. In Sec. V, we show the evolution of energy spectrum and spin gap when tuning the parameter crossing the phase boundary. Finally, in Sec. VI, we summarize our main results and discuss open questions.

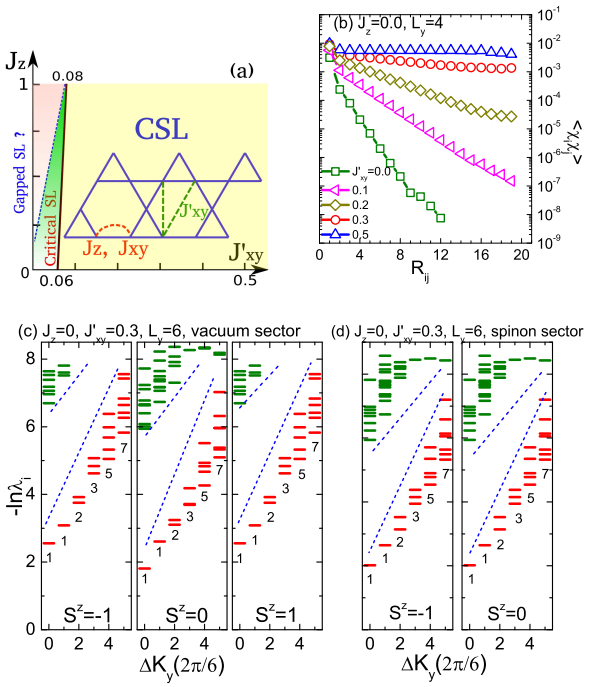

FIG. 1: (color online) (a) Schematic phase diagram of the spin-$1/2$ kagome model with Hamiltonian Eq. (1), where both the CSL and a critical SL with gapless singlet excitations are identified. The gapped SL[31] may exist neighboring with the critical SL. (b) Log-linear plot of chiral correlation $\langle \chi_i \chi_j \rangle$ versus the distance of triangles R_{ij} along the x direction for the ground state in the vacuum sector. (c) and (d) are the ES of the groundstates obtained using iDMRG in the vacuum and spinon sectors, respectively. λ_i is the eigenvalue of reduced density matrix.

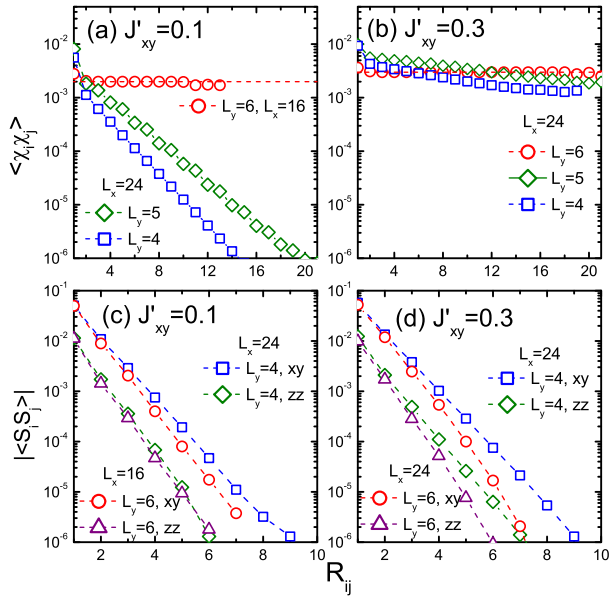

FIG. 2: (color online) (a) and (b) are the chiral correlations for the XY model ($J_z = 0$) with $J'_{xy} = 0.1$ and 0.3 on the cylinders with $L_y = 4, 5, 6$. (c) and (d) are the spin correlations of the xy component $|\langle S^x_i S^x_j + S^y_i S^y_j \rangle|$ and the zz component $|\langle S^z_i S^z_j \rangle|$ for the same systems with $L_y = 4$ and 6.

II. CHIRAL SPIN LIQUID PHASE

CSL is a TRS-broken SL phase which can be identified by various characteristic properties. First, CSL is a topological ordered state that hosts two-fold topological degenerate groundstates[41]. The ES for these two states, labeled by the quantum number total S^z of the half system, and their relative momentum quantum number along the y direction Δk_y[69,70], are shown in Figs. 1(c) and 1(d). The leading ES has the robust degeneracy pattern $\{1, 1, 2, 3, 5, 7\}$ with increasing Δk_y in each S^z sector, which follows the chiral $SU(2)_1$ Wess-Zumino-Witten conformal field theory description of the $\nu = 1/2$ FQH state[71] as the fingerprint for the emergence of the CSL[72]. The spectra of the vacuum and spinon sectors are symmetric about $S^z = 0$ and $-\frac{1}{2}$ respectively, indicating a spin-$\frac{1}{2}$ spinon at each end of cylinder in the spinon sector. The chiral edge spectrum is robust in different system

sizes (with the counting $\{1,1,2,3\}$ for the four momentum quantum numbers in the $L_y = 4$ system. See Supplemental Material[68]).

Second, CSL breaks TRS but preserves lattice symmetries, which can be detected by the chiral order parameter $\chi_i = (S_{i_1} \times S_{i_2}) \cdot S_{i_3}$ $(i_1, i_2, i_3 \in \triangle_i(\triangledown_i)$ triangle)[45]. As shown in Fig. 1(b) of the chiral correlations $\langle \chi_i \chi_j \rangle$ between the up-triangles i and j as a function of distance R_{ij} (for a system with $L_x = 24, L_y = 4$), the chiral correlations are enhanced gradually and appear to approach finite values at large distance for larger $J'_{xy} \sim 0.3$, which indicates the emerging long-range chiral order that characterizes the spontaneous TRS breaking. We also find that the chiral correlations grow with increasing system width for $J'_{xy} > 0.06$. As shown in Figs. 2(a) and 2(b), at $J'_{xy} = 0.1$, the chiral correlations decay exponentially to vanish at $L_y = 4$, while the chiral correlation is strongly enhanced for $L_y = 5$ system. As we increase the system width to $L_y = 6$, $\langle \chi_i \chi_j \rangle$ is very flat with a value near independent of R_{ij} at large distance. At $J'_{xy} = 0.3$, long-range chiral correlations are found for all system sizes. As shown in Figs. 2(c) and 2(d), in sharp contrast to the long-range chiral correlations, both the spin correlations of the xy component $|\langle S^x_i S^x_j + S^y_i S^y_j \rangle|$ and the zz component $|\langle S^z_i S^z_j \rangle|$ exhibit the exponential decay behavior for both system widths $L_y = 4$ and 6, indicating the vanished conventional spin order.

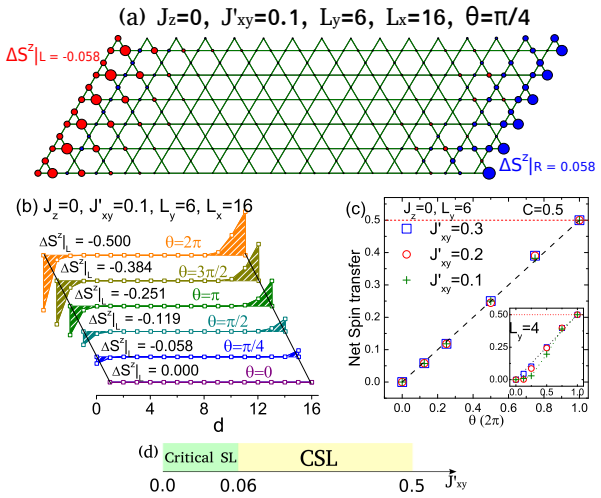

FIG. 3: (color online) (a) Spin magnetization $\langle S^z_{x,y} \rangle$ at $R_i = (x, y)$ after adiabatically inserting a flux $\theta = \pi/4$. The area of the circle is proportional to the amplitude of $\langle S^z_{x,y} \rangle$. The blue (red) color represents the positive (negative) $\langle S^z_{x,y} \rangle$. (b) Accumulated spin magnetization $\langle S^z_x \rangle = \sum_y \langle S^z_{x,y} \rangle$ in each column with inserting flux. (c) Net spin transfer $\Delta S^z|_{\text{edge}}$ as a function of θ on $L_y = 6$ cylinder. The inset shows the results on $L_y = 4$ cylinder. (d) Phase diagram of the XY kagome model ($J_z = 0$).

III. FRACTIONAL QUANTIZATION OF TOPOLOGICAL CHERN NUMBER

To reveal the full topological nature of the CSL phase, we perform the flux insertion simulation to obtain the topological Chern number[41]. By adiabatically inserting flux θ, we find that the nonzero spin-z polarization start to build up at both edges of cylinder. One example ($\theta = \pi/4$) is shown in Fig. 3(a). The net spin-z near boundaries grows monotonically with increasing θ as shown in Fig. 3(b), which is equivalent to the spin being pumped from the left edge to the right edge without accumulating in the bulk. As shown in Fig. 3(c), the linear spin pump behavior for $L_y = 6$ cylinder leads to a quantized net spin transfer $\Delta S^z|_{\text{edge}} = 0.500$ at $\theta = 2\pi$ and a quantized Chern number $C = 1/2$, fully characterizing the state as the $\nu = 1/2$ FQH state[41,47,73]. For the system with $L_y = 4$ as shown in the inset of Fig. 3(c), we find some finite size effect as the spin pump initially is zero for small θ, which jumps to the expected values of the linear pumping at a larger θ for $J'_{xy} = 0.1, 0.2$. However, the same topological quantization $C = 1/2$ is observed for $L_y = 4$ and $L_y = 5$ systems for CSL demonstrating the robust of the topological phase. The CSL is protected by the finite bulk excitation gap (shown later in Fig. 5) and grows stronger with increasing system width. Based on the quantized Chern number established for $L_y = 4 - 6$ cylinders with different geometries[68] and the conformal edge spectra, we find the CSL phase for $J'_{xy} \gtrsim 0.06$ as shown in the phase diagram Fig. 3(d) for $J_z = 0$.

IV. ENTANGLEMENT SPECTRUM FLOW

The CSL and the critical state can be understood based on the response of ES to inserted flux[74,75]. For a CSL at $J'_{xy} = 0.1$, as shown in Fig. 4, the eigenvalues of the reduced density matrix are degenerating about the $\pm S^z$ sectors at $\theta = 0$. By increasing θ, the spectrum lines in the positive S^z sectors flow up continuously, while those in the negative S^z sectors flow down (this is selected by the sign of Chern number due to spontaneous TRS breaking). At $\theta = 2\pi$, the eigenvalues in the $S^z = 0$ and $S^z = -1$ sectors become degenerate. As a result, after inserting a flux quantum, a net spin transfer $\Delta S|_L = \langle S^z|_L \rangle = \sum_i \lambda_i S^z_i = -1/2$ (the sign may change in each DMRG result due to the spontaneous TRS breaking) is realized and the spectrum becomes symmetric about $S^z = -1/2$. Thus the ES flow directly detects the gapless feature in the edge spectrum through inserting flux. By inserting 4π flux, the ES continues to flow and, it becomes symmetric about $S^z = -1$ at $\theta = 4\pi$, indicating two spinons have been transferred from the left edge to the right edge while the bulk of the system goes back to the vacuum sector. Furthermore, once the phase transition takes place, the ground-state wavefunction recovers TRS, and all the low-lying entanglement states become real states coming from the mixing between eigenstates with opposite chiralities. Correspondingly, the edge states with opposite chiralities also mix and merge into the bulk and become the low energy gapless excitations in the bulk[76].

V. LOW-ENERGY EXCITATIONS

We first study the evolution of the low-energy singlet excitations in the $S^z = 0$ sector as a function of J'_{xy} for the XY model ($J_z = 0$). As shown in Fig. 5(a) of the spectrum for 36-site torus system in $k = (0,0)$ sector, we find two low-energy near degenerate groundstates separated by a finite singlet gap E_s from higher energy excitations in the CSL phase at the large $J'_{xy} \simeq 0.2$ side. With decreasing J'_{xy}, E_s reduces, which collapses to the ground state at $J'_{xy} \sim 0 - 0.05$. Thus the quantum phase transition from the CSL to the TRS preserving state is driven by such a neutral excitation gap closing. For comparison, we also obtain the triplet gap E_T in the DMRG calculations using torus systems with $N = 3 \times 4 \times 3$, $3 \times 4 \times 4$ and $3 \times 4 \times 8$ as shown in Fig. 5(b)[77]. E_T drops with reducing J'_{xy} and it becomes much smaller for $N = 96$ system when approaching $J'_{xy} = 0$. Finite size scaling[68] indicates that the spin gap vanishes in the thermodynamic limit. Thus, our results indicate that the critical state is centered near $J'_{xy} = 0$, with the vanishing spin singlet and triplet gaps. The appearance of low-energy singlet excitations below the finite-size spin gap can be understood as the gapless neutral mode for the topological quantum phase transition[65,66], which necessarily exists for such a transition.

Furthermore, we examine the low energy spectra of the NN XXZ model ($J'_{xy} = 0$) on $N = 3 \times 4 \times 3$ torus. As shown in Figs. 5(c-e) for $J_z = 0.0, 0.5$ and 1.0, we find near continuous low energy excitations[78] collapsing together below the spin triplet gap, which implies the gapless singlet excitations in the whole critical SL region. The structure of the energy spectra remains very similar, however, the finite size spin gap increases with the growing J_z. The finite size scaling using different torus systems indicates that the spin gap behavior is quite different for the NN XY model (which vanishes) and the Heisenberg model, while in the latter the spin excitation may remain to be gapped consistent with the gapped Z_2 SL there[68]. We summarize our results as the phase diagram with varying J_z and J'_{xy} in Fig. 1. While we determine the phase boundary of CSL accurately, we cannot determine the precise phase boundary of the critical SL at the smaller J'_{xy} side due to the limited system width we can access in DMRG simulations. The gapped SL[31] may exist neighboring with the critical SL close to the NN Heisenberg model. Very recently, by using the variational Monte Carlo technique, Ref.[79] found that $U(1)$ gapless spin liquid and critical behavior is more robust near the XY limit, which is consistent with our DMRG calculation here.

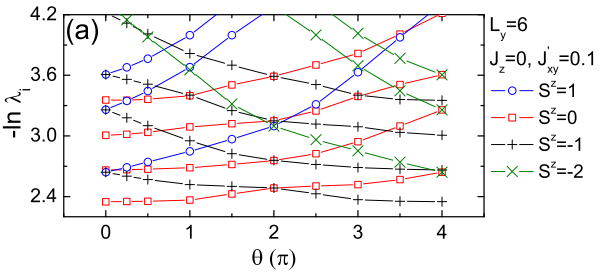

FIG. 4: (color online) ES flow with inserting flux θ for $J_z = 0, J'_{xy} = 0.1$ on a $L_y = 6, L_x = 16$ cylinder system obtained using iDMRG.

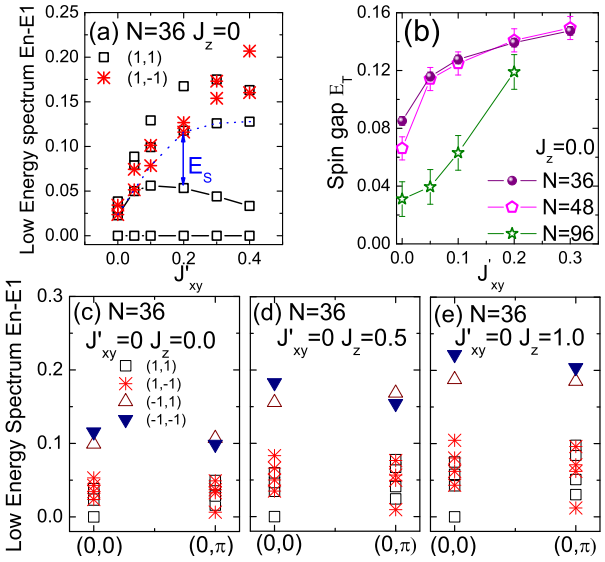

FIG. 5: (color online) (a) Evolution of ED low-energy spectrum in the $k = (0,0)$ sector with J'_{xy} for the XY model on the $3 \times 3 \times 4$ torus. The singlet gap between the lowest two groundstates and higher-energy states is denoted as E_s. (b) J'_{xy} dependence of spin gap E_T for the XY model on $3 \times 3 \times 4$, $3 \times 4 \times 4$, and $3 \times 4 \times 8$ tori. Low-energy spectrum of the NN XXZ model ($J'_{xy} = 0$) at $k = (0,0)$ and $(0,\pi)$ sectors for (c) $J_z = 0.0$, (d) $J_z = 0.5$, and (e) $J_z = 1.0$ on the $3 \times 3 \times 4$ torus. The label $(\pm 1, \pm 1)$ denote the quantum numbers related to spin inversion and lattice $\pi-$rotation symmetries.

VI. SUMMARY AND DISCUSSIONS

We identify a TRS broken CSL phase with a small perturbation $J'_{xy} \simeq 0.06$ in the $J_{xy} - J'_{xy}$ XY model, while the NN XY model is in a critical phase adjacent to the CSL with vanishing spin singlet and triplet excitation gaps. Our CSL extends to small J'_{xy} based on finite-size scaling of wider systems, which is different from a recent work mainly based on $L_y = 4$ DMRG results[49]. Furthermore, by studying the evolution of ES crossing the quantum phase transition and spin gap, we identify that the quantum phase transition takes place through the coupling and mixing of the chiral states with opposite chiralities, which naturally lead to a critical state with TRS and gapless neutral excitations for NN XY model. The quantum phase transition appears to be very smooth, which is driven by the continuous closing of the gap for spin singlet excitations. Furthermore, the gapped Z_2 SL[31] may develop on larger systems in the NN model near the Heisenberg point, through opening the vison gap from the gapless neutral excitations outside the critical SL.

VII. ACKNOWLEDGEMENT

We hope to thank L. Balents, F. D. M. Haldane, L. Fu, P. A. Lee, T. Senthil, Z. Y. Weng, and especially X. G. Wen for stimulating discussions. We also thank Y. C. He and L. Cincio for their insightful discussions about developing infinite DMRG algorithm. This research is supported by the U.S. Department of Energy, Office of Basic Energy Sciences under grant No. DE-FG02-06ER46305 (W.Z., D.N.S.), the National Science Foundation through grants DMR-1408560 (S.S.G).

Appendix A: Infinite DMRG algorithm

We use both finite and infinite density matrix renormalization group (iDMRG)[80] to study this model. In the iDMRG algorithm, we first start from a small system size. Then we insert one column in the center and optimize the energy by sweeping the inserted column. After the optimization, we absorb the new column into the original existing system and get the new boundary Hamiltonians. We repeat the inserting, optimizing and absorbing procedure until the energy convergence is achieved. Compared with the finite DMRG simulation, iDMRG grows the lattice by one column at each iteration and only sweeps the inserted column, thus the computation cost is significantly reduced. iDMRG is especially efficient to deal with the gapped topological order system, which allows us to obtain the ground states with well-defined anyonic flux as first proposed in Ref.[81]. In our work, we have confirmed that the iDMRG obtains the fixed-point ground state wavefunction in the center of cylinder that is the same as that obtained from the finite DMRG simulations (the same energy and the identical entanglement spectrum within the numerical error.). We extensively use the iDMRG for entanglement spectrum calculations. However, for the chiral correlation function involving six spin operators, we use finite DMRG to obtain more converged results. The topological Chern number is the total Berry phase associated with the chirality of the system, which is robust and easy to calculate due to the topological invariant. We obtain the same results for Chern number using either iDMRG or finite DMRG.

In our DMRG calculations, we ensure the convergence of results by checking the truncation error, and measuring the physical quantities such as energy, correlation functions, Chern number, and entanglement spectrum with increasing kept states to confirm whether the quantities are converged. On the $L_y = 6$ cylinder, we find that the topological properties such as Chern number and chiral edge spectrum are easier to converge and are converged in our calculations, which are used as our primary quantities to identify the chiral spin liquid. Chiral correlation functions are harder to converge, so we keep increasing optimal states to make sure the obtained correlation functions are almost invariant with growing kept states. In the parameter points near the transition, we have worked with shorter system ($L_x = 16$) to keep up to $m = 14000$ states for converged chiral correlations (shown in Fig.2 of main text).

Around $J'_{xy} = 0$ for the possible gapless regime, it is harder to reach the convergence. So we focus on the smaller torus systems ($3\times3\times4$, $3\times4\times4$, and $3\times4\times8$) and our spin gap is converged with increasing the number of states to $m = 10000$.

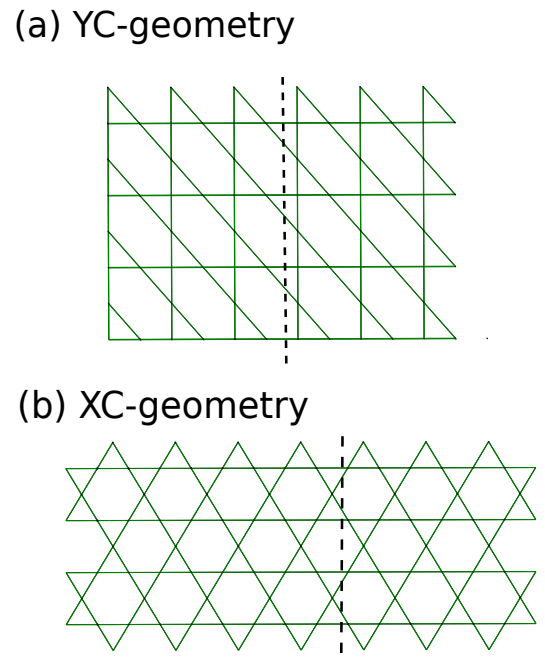

FIG. 6: (color online) Kagome cylinder on (a) YC geometry and (b) XC geometry. The cylinders are closed in the y direction and opened in the x direction.

Appendix B: Entanglement spectrum on XC geometry

There are two kinds of cylinder geometries on kagome lattice often being studied in DMRG as YC-geometry in Fig. 6(a) and XC-geometry in Fig. 6(b). In the main text, the demonstrated results are all based on YC-geometry. Here we show that the entanglement spectrum and the spectrum flow shown on YC-geometry are robust and insensitive to the lattice geometry. In Fig. 7, we demonstrate the entanglement spectrum flow for $J_z = 0, J'_{xy} = 0.1$ on $L_y = 6$ XC-geometry. The features of the spectrum flow are consistent with the results on YC-geometry shown in Fig. 4 of the main text. The eigenvalues in the $S^z = 1$ and $S^z = -1$ sectors are degenerate at $\theta = 0$. By increasing flux θ, the eigenvalues in $S^z = 1$ sector flow up while those in $S^z = -1$ sector flow down continuously. At $\theta = 2\pi$, the eigenvalues in the $S^z = 0$ and $S^z = -1$ sectors become degenerate, which results in a fractionally quantized Chern number $C = 1/2$. Thus, the phase diagram shown in the main text is robust for different geometries.

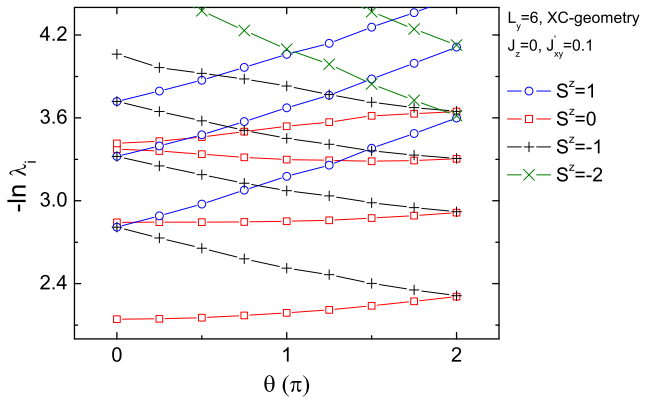

FIG. 7: (color online) Entanglement spectrum flow for $J_z = 0.0, J'_{xy} = 0.1$ on $L_y = 6$ XC cylinder, which is obtained by keeping 3000 states using iDMRG.

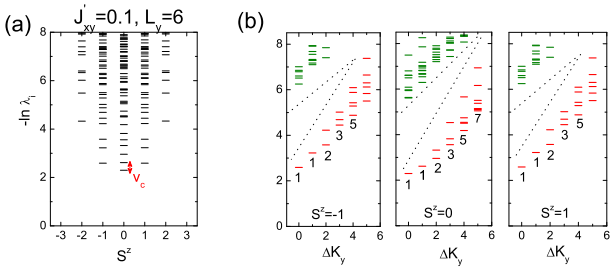

FIG. 8: (color online) (a) Entanglement spectrum for $J_z = 0.0, J'_{xy} = 0.1$ on $L_y = 6$ YC cylinder, which is obtained by keeping 3000 states. The red arrow denoted as v_c indicates the two lowest values in $k = 0$ and $2\pi/L_y$ sectors that are used to calculate the chiral velocity. (b) Near degenerating pattern for the low-lying entanglement spectra with different relative momentum Δk_y and total spin S^z for the same system in (a). Δk_y is in unit of $2\pi/6$. All results are obtained using iDMRG.

Appendix C: Chiral Velocity From Entanglement Spectrum and its Evolution

Entanglement spectrum resembles the edge excitation spectrum that can be viewed as a fingerprint of topological order. In the main text, we show the entanglement spectrum at $J_z = 0.0, J'_{xy} = 0.3$ in Fig. 1(c) and 1(d). The characteristic chiral edge spectrum indicates the chiral spin liquid (CSL) state. Here we show the spectrum at $J_z = 0.0, J'_{xy} = 0.1$ on YC-geometry, which is closer to the phase boundary $J'_{xy} \simeq 0.06 J_{xy}$. As shown in Fig. 8, the entanglement spectrum also exhibits the degeneracy pattern $\{1,1,2,3,5,...\}$ consistent with the CSL state.

Entanglement spectrum gives not only the characteristic degeneracy pattern of the edge excitation, but also the edge-mode velocity[82]. In the conformal field theory, the edge-mode of the Laughlin state is described by a single branch of chiral charged bosons. The velocity of the charged bosons v_c is not an universal quantity as it depends on the microscopic interaction and edge confinement. In the cylinder geometry, we can define v_c through the lowest values of entanglement spectrum with edge momentum $k = 0$ and $k = \frac{2\pi}{L_y}$: $v_c = \frac{\Delta E}{\hbar \Delta k} = \frac{E_0(k=2\pi/L_y) - E_0(k=0)}{\hbar 2\pi/L_y}$, where $E_0(k) = min\{-ln\lambda(k)\}$ is the lowest eigenvalue with edge momentum k. Thus, from our results on YC-geometry, we have $\frac{v_c(J'_{xy}=0.1)}{v_c(J'_{xy}=0.3)} \approx 0.439$. Although the CSL state is still robust at $J'_{xy} = 0.1$, the edge-mode velocity is reduced compared to $J'_{xy} = 0.3$ in the deep CSL phase. With further decreasing J'_{xy}, we find that the difference of the lowest value between the momentum sectors $k = 0$ and $k = 2\pi/L_y$ continuously decreases before the quantum phase transition takes place. The reducing of chiral velocity obtained from entanglement spectrum is related with the drop of the bulk excitation gap with decreasing J'_{xy}, which is consistent with a very weakly first order transition or a continuous transition driven by the collapsing of the bulk gap and the destruction of the gapless edge states at the same time.

With decreasing J'_{xy}, the robust Chern number quantization and the spectrum flow persist to $J'_{xy} \simeq 0.06$. By following the evolution of the ES, we find that the CSL is becoming less strong at the smaller J'_{xy}, where the chiral velocity v_c diminishes with decreasing J'_{xy}. As illustrated in Fig. 9(a) and (b), we observe that the ES as a function of quantum number S^z before and after the phase transition appear to be similar at $J'_{xy} = 0.1$ and 0.0. However, they are significantly different in momentum space. The spectrum for $J'_{xy} = 0.1$ preserves the same robust conformal chiral edge spectrum as demonstrated in Fig. 8 with many entanglement eigenstates carrying nonzero k_y. Once the phase transition takes place, the ground-state wavefunction has TRS, and the low-lying entanglement states shown in Fig. 9(b) have the momentum quantum number k_y either 0 or π if they are nondegenerate, which comes from the mixing between eigenstates with opposite chiralities. Furthermore, these low-lying eigenstates do not respond to the inserted flux. The mixing of entanglement states with opposite chiralities illustrates what happens to the physical edge states. These edge states with opposite chiralities also mix and merge into the bulk and become the low energy gapless excitations in the bulk. These observations are consistent with the theoretical prediction for the quantum phase transition between two states with different Chern numbers[65,66]. Interestingly, the ES for the NN kagome Heisenberg model in Fig. 9(c) is similar to the one of the NN XY model.

Appendix D: Chiral Spin Liquid phase when $J_z \neq 0$

In the main text, we show the entanglement spectrum of the CSL phase in the XY model ($J_z = 0$). Here, to demonstrate the CSL phase can extend from $J_z = 0$ to nonzero J_z, we show the entanglement spectrum for two more parameter points as shown in Fig. 10. It is found that the leading ES has the robust degeneracy pattern $\{1, 1, 2, 3, 5, \cdots\}$ with increasing Δk_y in each S^z sector. The entanglement spectrum signals that the characteristic edge mode counting of the CSL phase. We also show that the entanglement spectrum has the same characteristic feature for $L_y = 4$ system inside the CSL

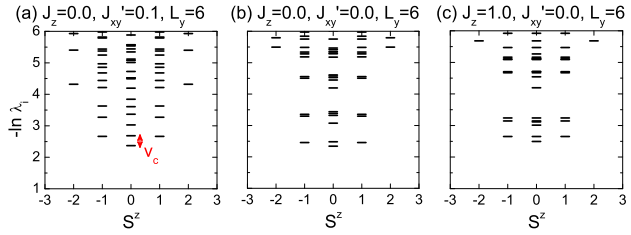

FIG. 9: (color online) ES for (a) $J_z = 0.0, J'_{xy} = 0.1$, (b) $J_z = 0.0, J'_{xy} = 0.0$, and (c) $J_z = 1.0, J'_{xy} = 0.0$. The arrow denoted by v_c in (b) indicates the two lowest eigenvalues in the $S^z = 0$ sector which are used to calculate the chiral edge-mode velocity.

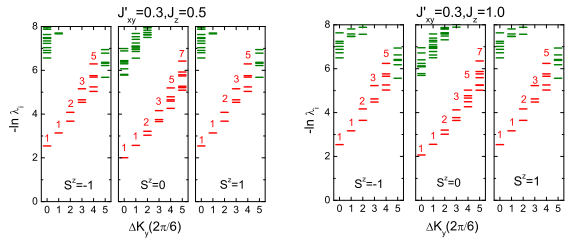

FIG. 10: (color online) Entanglement spectrum for (Left) $J_z = 0.5, J'_{xy} = 0.3$ and (Right) $J_z = 1.0, J'_{xy} = 0.3$ on $L_y = 6$ YC cylinder, which is obtained by keeping 1600 states in iDMRG calculations. Near degenerating pattern for the low-lying entanglement spectra with different relative momentum Δk_y and total spin S^z for the same system in main text. Δk_y is in unit of $2\pi/6$.

phase ($J'_{xy} = 0.3$), as shown in Fig. 11. In the main text, we determine the regime of CSL phase in the phase diagram based on the characteristic entanglement spectrum and the robust Chern number calculations.

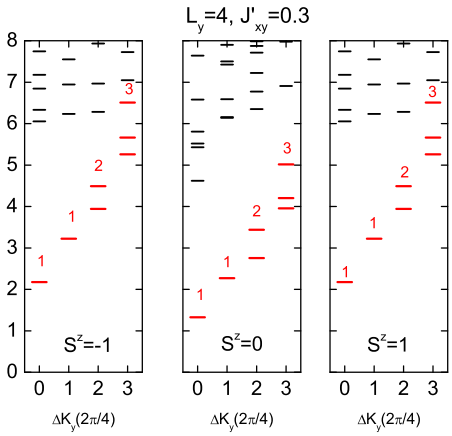

FIG. 11: (color online) Entanglement spectrum for $J'_{xy} = 0.3$ on the $L_y = 4$ YC cylinder, which is obtained using iDMRG. Δk_y is in unit of $2\pi/4$. The low-lying entanglement spectra have the degeneracy pattern $\{1, 1, 2, 3\}$.

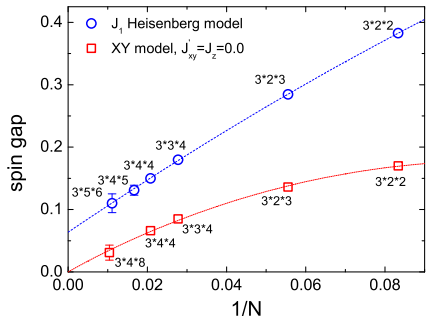

FIG. 12: (color online) Size dependence of the spin gap obtained on the torus systems with $N = 12$ to 96. The blue circles and red squares denote the gap of the pure Heisenberg kagome model and the pure XY kagome model, respectively. Both data are fitted using the formula $\Delta_T = \alpha/N + \beta/N^{3/2} + \gamma/N^2$.

Appendix E: Spin gap on torus system

From finite size scaling of the spin gap for torus system with different geometry shown in Fig. 12, we find that the spin gap for the NN XY model scales to zero. The spin gap reduces with the system sites N, where we used systems of $N = 12$ to $N = 3 \times 8 \times 4$ for the NN XY model and $N = 12$ to $N = 3 \times 5 \times 6$ for the NN Heisenberg model. The spin gap in XY case extrapolates to zero no matter if we use 2D-like cluster or more 1D-like cluster. For the NN Heisenberg model, the spin gap scales to a finite value, indicating the development of a gapped SL.

[1] L. Balents, Nature **464**, 199 (2010).
[2] X. G. Wen, Phys. Rev. B **40**, 7387 (1989).
[3] X. G. Wen and Q. Niu, Phys. Rev. B **41**, 9377 (1990).
[4] X. G. Wen, Int. J. Mod. Phys. B **4**, 239 (1990).
[5] X. Chen, Z. C. Gu, and X. G. Wen, Phys. Rev. B **82**, 155138 (2010).
[6] P. W. Anderson, Science **235**, 1196 (1987).
[7] D. S. Rokhsar and S. A. Kivelson, Phys. Rev. Lett. **61**, 2376 (1988).
[8] N. Read and S. Sachdev, Phys. Rev. Lett. **66**, 1773 (1991).
[9] X. G. Wen, Phys. Rev. B **44**, 2664 (1991).
[10] T. Senthil and M. P. A. Fisher, Phys. Rev. B **62**, 7850 (2000); Phys. Rev. Lett. **86**, 292 (2001).
[11] R. Moessner and S. L. Sondhi, Phys. Rev. Lett. **86**, 1881 (2001).
[12] L. Balents, M. P. A. Fisher, and S. M. Girvin, Phys. Rev. B **65**, 224412 (2002).
[13] T. Senthil and O. I. Motrunich, Phys. Rev. B **66**, 205104 (2002).
[14] O. I. Motrunich and T. Senthil, Phys. Rev. Lett. **89**, 277004 (2002).
[15] D. N. Sheng and L. Balents, Phys. Rev. Lett. **94**, 146805 (2005).
[16] P. A. Lee, N. Nagaosa, and X. G. Wen, Rev. Mod. Phys. **78**, 17 (2006).
[17] A. Kitaev, Ann. Phys. (N.Y.) **321**, 2 (2006).
[18] D. F. Schroeter, E. Kapit, R. Thomale, and M. Greiter, Phys. Rev. Lett. **99**, 097202 (2007).
[19] P. A. Lee, Science **321**, 1306 (2008).
[20] S. V. Isakov, M. B. Hastings, R. G. Melko, Nat. Phy. **7**, 772 (2011).
[21] H. Yao and S. A. Kivelson, Phys. Rev. Lett. **108**, 247206 (2012).
[22] F. Wang, Phys. Rev. B **82**, 024419 (2010).
[23] Y. M. Lu and Y. Ran, Phys. Rev. B **84**, 024420 (2011).
[24] B. K. Clark, D. A. Abanin, and S. L. Sondhi, Phys. Rev. Lett. **107**, 087204 (2011).
[25] H. C. Jiang, H. Yao, and L. Balents, Phys. Rev. B **86**, 024424 (2012).
[26] R. Ganesh, J. vandenBrink, and S. Nishimoto, Phys. Rev. Lett. **110**, 127203 (2013).
[27] Z. Y. Zhu, D. A. Huse, and S. R. White, Phys. Rev. Lett. **110**, 127205 (2013).
[28] S. S. Gong, D. N. Sheng, O. I. Motrunich, and M. P. A. Fisher, Phys. Rev. B **88**, 165138 (2013).
[29] S. S. Gong, W. Zhu, D. N. Sheng, O. I. Motrunich, and M. P. A. Fisher, Phys. Rev. Lett. **113**, 027201 (2014).
[30] H. C. Jiang, Z. Y. Weng, and D. N. Sheng, Phys. Rev. Lett. **101**, 117203 (2008).
[31] S. Yan, D. Huse, and S. R. White, Science **332**, 1173 (2011).
[32] S. Depenbrock, I. P. McCulloch, and U. Schollwöck, Phys. Rev. Lett. **109**, 067201 (2012).
[33] H. C. Jiang, Z. H. Wang, and L. Balents, Nat. Phy. **8**, 902 (2012).
[34] A. Kitaev, J. Preskill, Phys. Rev. Lett. **96**, 110404 (2006).
[35] M. Levin, X. G. Wen, Phys. Rev. Lett. **96**, 110405 (2006).
[36] L. Balents, M. P. A. Fisher, and C. Nayak, Phys. Rev. B **60**, 1654 (1999).
[37] Y. C. He, D. N. Sheng, and Y. Chen, Phys. Rev. B **89**, 075110 (2014).
[38] Y. Ran, M. Hermele, P. A. Lee, and X. G. Wen, Phys. Rev. Lett. **98**, 117205 (2007).
[39] Y. Iqbal, F. Becca, and D. Poilblanc, Phys. Rev. B **84**, 020407(R) (2011).
[40] L. Messio, B. Bernu, and C. Lhuillier, Phys. Rev. Lett. **108**, 207204 (2012).
[41] S. S. Gong, W. Zhu, and D. N. Sheng, Sci. Rep. **4**, 6317 (2014).
[42] Y. C. He, D. N. Sheng, and Y. Chen, Phys. Rev. Lett. **112**, 137202 (2014).
[43] R. B. Laughlin, Phys. Rev. Lett. **50**, 1395 (1983).
[44] V. Kalmeyer and R. B. Laughlin, Phys. Rev. Lett. **59**, 2095 (1987).
[45] X. G. Wen, F. Wilczek, and A. Zee, Phys. Rev. B **39**, 11413 (1989).
[46] K. Yang, L. K. Warman, and S. M. Girvin, Phys. Rev. Lett. **70**, 2641 (1993).
[47] F. D. M. Haldane and D. P. Arovas, Phys. Rev. B **52**, 4223 (1995).
[48] J. W. Mei and X. G. Wen, arXiv:1407.0869.
[49] Y. C. He and Y. Chen, Phys. Rev. Lett. **114**, 037201 (2015).
[50] B. Bauer, L. Cincio, B. P. Keller, M. Dolfi, G. Vidal, S. Trebst, A. W. W. Ludwig, arXiv:1401.3017.
[51] M. Barkeshli, arXiv:1307.8194.
[52] Y. Shimizu, K. Miyagawa, K. Kanoda, M. Maesato, and G. Saito, Phys. Rev. Lett. **91**, 107001 (2003).
[53] Y. Kurosaki, Y. Shimizu, K. Miyagawa, K. Kanoda, and G. Saito, Phys. Rev. Lett. **95**, 177001 (2005).
[54] T. Itou, A. Oyamada, S. Maegawa, M. Tamura, and R. Kato, Phys. Rev. B **77**, 104413 (2008).
[55] P. Mendels, F. Bert, M. A. de Vries, A. Olariu, A. Harrison, F. Duc, J. C. Trombe, J. S. Lord, A. Amato, and C. Baines, Phys. Rev. Lett. **98**, 077204 (2007).
[56] J. S. Helton, K. Matan, M. P. Shores, E. A. Nytko, B. M. Bartlett, Y. Yoshida, Y. Takano, A. Suslov, Y. Qiu, J.-H. Chung, D. G. Nocera, and Y. S. Lee, Phys. Rev. Lett. **98**, 107204 (2007).
[57] M. A. de Vries, J. R. Stewart, P. P. Deen, J. Piatek, G. N. Nilsen, H. M. Ronnow, and A. Harrison, Phys. Rev. Lett. **103**, 237201 (2009).
[58] B. Fåk, E. Kermarrec, L. Messio, B. Bernu, C. Lhuillier, F. Bert, P. Mendels, B. Koteswararao, F. Bouquet, J. Ollivier, A. D. Hillier, A. Amato, R. H. Colman, and A. S. Wills, Phys. Rev. Lett. **109**, 037208 (2012).
[59] T. H. Han, J. S. Helton, S. Chu, D. G. Nocera, J. A. Rodriguez-Rivera, C. Broholm, and Y. S. Lee, Nature **492**, 7429 (2012).
[60] L. Clark, J. C. Orain, F. Bert, M. A. De Vries, F. H. Aidoudi, R. E. Morris, P. Lightfoot, J. S. Lord, M. T. F. Telling, P. Bonville, J. P. Attfield, P. Mendels, and A. Harrison, Phys. Rev. Lett. **110**, 207208 (2013).
[61] J. Alicea, O. I. Motrunich, and M. P. A. Fisher, Phys. Rev. Lett. **95**, 247203 (2005).
[62] S. Ryu, O. I. Motrunich, J. Alicea, and M. P. A. Fisher, Phys. Rev. B **75**, 184406 (2007).
[63] C. Wang and T. Senthil, arXiv:1407.7533.
[64] S.-S. Gong, W. Zhu, L. Balents, and D. N. Sheng, Phys. Rev. B **91**, 075112 (2015).
[65] I. A. McDonald and F. D. M. Haldane, Phys. Rev. B **53**, 15845 (1996).
[66] X. G. Wen, Phys. Rev. Lett. **84**, 3950 (2000).
[67] S. R. White, Phys. Rev. Lett. **69**, 2863 (1992).
[68] See more information in Supplemental Material.
[69] L. Cincio and G. Vidal, Phys. Rev. Lett. **110**, 067208 (2013).
[70] Michael P. Zaletel, Roger S. K. Mong, and Frank Pollmann, Phys. Rev. Lett. **110**, 236801 (2013).
[71] P. Di Francesco, P. Mathieu, and D. Senechal, *Conformal Field Theory* (Springer, New York, 1997), Chap. 15.6.
[72] H. Li and F. D. M. Haldane, Phys. Rev. Lett. **101**, 010504 (2008).
[73] Y. Hatsugai, Phys. Rev. Lett. **71**, 3697 (1993).
[74] W. Zhu, S. S. Gong, and D. N. Sheng, J. Stat. Mech. 2014 (8), P08012.
[75] A. G. Grushin, J. Motruk, M. P. Zaletel, and F. Pollmann,

arXiv:1407.6985.
[76] X. L. Qi, H. Katsura, A. W. W. Ludwig, Phys. Rev. Lett. **108**, 196402 (2012).
[77] While one cannot get a few low energy singlet excitations in DMRG accurately, one can obtain the triplet gap E_T by targeting the ground states in the different total S^z sectors separately.
[78] C. Waldtmann, H. U. Everts, B. Bernu, C. Lhuillier, P. Sindzingre, P. Lecheminant, L. Pierre, Eur. Phys. J. B **2**, 501 (1998).
[79] W. J. Hu, S. S. Gong, F. Becca and D. N. Sheng, arXiv. 1505.06276.
[80] I. P. McCulloch, arXiv:0804.2509.
[81] L. Cincio and G. Vidal, Phys. Rev. Lett. **110**, 067208 (2013).
[82] Z. X. Hu, E. H. Rezayi, X. Wan, and K. Yang, Phys. Rev. B **80**, 235330 (2009).